

# StableAML: Machine Learning for Behavioral Wallet Detection in Stablecoin Anti-Money Laundering on Ethereum

Luciano Juvinski<sup>a</sup>      Haochen Li<sup>a</sup>      Alessio Brini<sup>a</sup>  
luciano.silva@duke.edu    haochen.li2@duke.edu    alessio.brini@duke.edu

<sup>a</sup>*Duke University Pratt School of Engineering, 305 Teer Engineering Building, Box 90271, Durham, NC 27708, USA*

**Keywords:** Anti-Money Laundering, Stablecoins, Blockchain Analytics, Know Your Transaction, Machine Learning.

## Abstract

Global illicit fund flows exceed an estimated \$3.1 trillion annually, with stablecoins emerging as a preferred laundering medium due to their liquidity. While decentralized protocols increasingly adopt zero-knowledge proofs to obfuscate transaction graphs, centralized stablecoins remain critical "transparent choke points" for compliance. Leveraging this persistent visibility, this study analyzes an Ethereum dataset and uses behavioral features to develop a robust AML framework. Our findings demonstrate that domain-informed tree ensemble models achieve higher Macro-F1 score, significantly outperforming graph neural networks, which struggle with the increasing fragmentation of transaction networks. The model's interpretability goes beyond binary detection, successfully dissecting distinct typologies: it differentiates the complex, high-velocity dispersion of cybercrime syndicates from the constrained, static footprints left by sanctioned entities. This framework aligns with the industry shift toward deterministic verification, satisfying the auditability and compliance expectations under regulations such as the EU's MiCA and the U.S. GENIUS Act while minimizing unjustified asset freezes. By automating high-precision detection, we propose an approach that effectively raises the economic cost of financial misconduct without stifling innovation.

# 1 Introduction

Most forms of organized criminal activity have a financial component. Whether arising from corruption, trafficking, cyber-enabled fraud, or terrorist financing, illicit proceeds must be concealed, moved, and eventually reintegrated into the legitimate economy. This dependence on financial flows makes money laundering the cornerstone of criminal enterprises. In 2024, an estimated \$3.1 trillion in illicit funds flowed through the global financial system, fueling a shadow economy outside regulatory control (Verafin, 2024).

Blockchain money laundering mirrors the traditional placement, layering, and integration stages of financial crime but occurs at a significantly higher speed. An estimated \$51 billion was laundered through cryptocurrencies in 2024, representing approximately 0.14% of all on-chain transactions<sup>1</sup>, which totaled \$9 trillion. Crypto-based laundering typically involves injecting illicit funds, obscuring their origins through complex and multi-hop transaction paths<sup>2</sup>, and ultimately reintegrating them into the legitimate economy. This environment exhibits a dual nature: while public ledgers provide technical transparency by making transaction histories visible, they simultaneously preserve pseudonymity by linking activity only to cryptographic addresses. Paradoxically, rather than preventing illicit practices, this open and permissionless architecture has enabled increasingly sophisticated obfuscation techniques involving decentralized exchanges, token swaps, and cross-chain bridges (Lin et al., 2023; Griffin et al., 2025). Within this ecosystem, stablecoins have emerged as central vehicles for value transfer. Stablecoins are cryptocurrencies engineered to maintain a stable value relative to an external reference, such as a fiat currency or commodity, typically through collateralization or algorithmic mechanisms. By reducing price volatility, they function as media of exchange and units of account within both centralized and decentralized financial infrastructures (Clark et al., 2019). Owing to these properties, stablecoins have become the dominant vehicle for illicit value transfer, accounting for over 84% of all verified crypto fraud volumes in 2025<sup>3</sup>, driven by their high liquidity, interoperability, and deep integration across exchanges, decentralized finance (DeFi) protocols, and payment rails.

The Ethereum blockchain plays a particularly important role due to its dominance in Web3<sup>4</sup> activity and its high incidence of security events. Tether (USDT) and Circle USD Coin (USDC) together processed over \$10 trillion in transfer volume in 2025<sup>5</sup>, exceeding the settlement activity of both Bitcoin and Ethereum combined (see Figure 1). Although these assets support legitimate financial activity, their rapid settlement, which often allows transactions to finalize within seconds rather than days, combined with borderless accessibility and inherent pseudonymity, makes them attractive for money laundering (Pochoer et al., 2023). Recent empirical findings further show that stablecoins are now the preferred medium for laundering and sanctions evasion, particularly following enforcement actions against obfuscation services such as mixer<sup>6</sup> protocols (Griffin et al., 2025).

---

<sup>1</sup><https://go.chainalysis.com/2025-Crypto-Crime-Report>

<sup>2</sup>A multi-hop transaction refers to the practice of routing funds through a sequence of intermediate wallet addresses before reaching a final destination, rather than a single direct transfer. In anti-money laundering contexts, this technique is commonly used to create a complex chain of custody, effectively distancing the funds from their illicit origin and complicating audit trails.

<sup>3</sup><https://www.trmlabs.com/reports-and-whitepapers/2026-crypto-crime-report>

<sup>4</sup>Web3 refers to a paradigm for web-based applications that leverages blockchain technology, smart contracts, and token-based economic mechanisms to enable decentralized execution and coordination. In contrast to Web 2.0 platforms, which typically rely on centralized intermediaries, Web3 applications allow users to interact through decentralized applications (dApps) in which control over digital assets is mediated by cryptographic keys rather than centralized authorities.

<sup>5</sup><https://visaonchainanalytics.com/transactions>

<sup>6</sup>Mixers are services designed to obscure transaction provenance by pooling funds from multiple users and redistributing them in a way that breaks the link between sender and recipient.

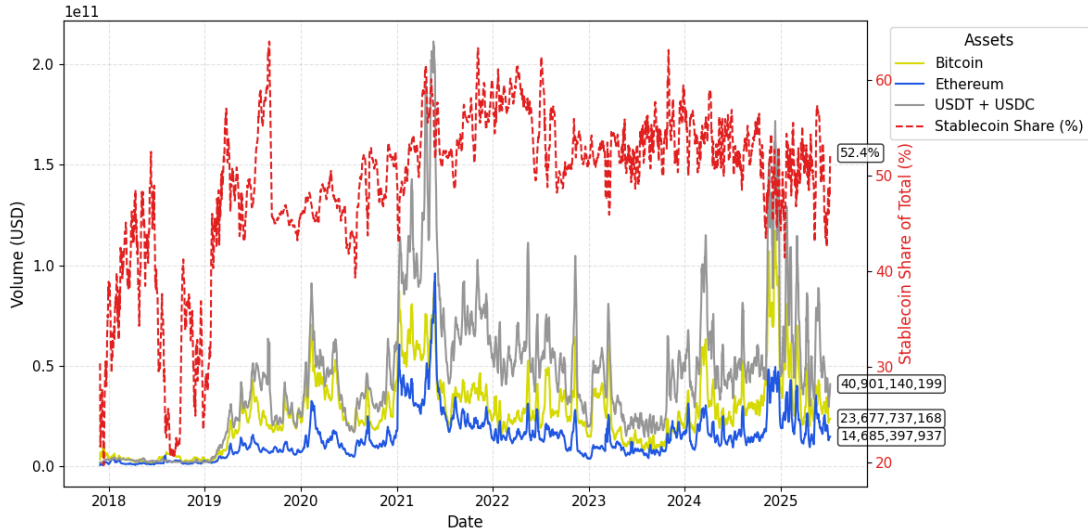


**Figure 1:** Historical transaction volumes for Bitcoin, Ethereum, and combined stablecoins.

Concurrent with these trends, stablecoin regulation is advancing rapidly across major jurisdictions. The EU’s Markets in Crypto-Assets (MiCA) Regulation (2023) and the U.S. GENIUS Act (2025) mandate that stablecoin issuers maintain full reserve backing, undergo independent audits, and comply with comprehensive Anti-Money Laundering (AML) requirements, while several Asian regulators have introduced comparable regimes. Among those, Singapore strengthened its oversight through the Payment Services Act and the 2023–2024 Stablecoin Regulatory Framework, while Hong Kong implemented its Stablecoin Issuer Regulatory Regime through recent amendments to the Anti-Money Laundering and Counter-Terrorist Financing Ordinance. China also regulates private stablecoin activity under the People’s Bank of China Digital Currency Framework linked to its ongoing digital yuan initiative.

In parallel with these regulatory efforts, major stablecoin issuers, such as Tether and Circle, have adopted wallet freezes, an enforcement mechanism in which the issuer leverages smart-contract privileges to prevent designated addresses from transferring, redeeming, or otherwise moving their tokens. Recent evidence shows that such freezes have immobilized over \$4 billion in USDT and more than \$1 billion in USDC, substantially increasing both the cost and the traceability of illicit transactions (Griffin et al., 2025). These freezes trap criminal funds on-chain. They also prompt offenders to add intermediary hops, routing funds through a sequence of additional wallets and services, to circumvent restrictions. This often results in longer and less traceable transaction paths. Collectively, these regulatory and enforcement developments underscore the growing effectiveness of policy-driven interventions. However, while these measures serve to raise the economic cost of financial crime, they simultaneously drive illicit actors toward increasingly sophisticated evasion strategies to bypass them. This adversarial evolution creates a critical need for scalable detection frameworks that continuously monitor and adapt to shifting laundering behaviors on the blockchain.

The core challenge is differentiating legitimate activities from illicit ones in high-throughput environments that process millions of transactions daily. Conventional rule-based systems, widely used in traditional finance, rely on static thresholds and deterministic heuristics such as flagging transfers above fixed monetary limits, detecting rapid bursts of activity, or blocking wallets previously labeled as high-risk. Although intuitive, these systems represent a staggering

inefficiency, producing false positive rates that exceed 95% (Liu et al., 2023). This operational failure imposes massive economic overheads, estimated at \$136.5 billion in annual compliance costs in Europe alone, yet intercepts only 0.1% of global criminal funds (Akartuna et al., 2022). Such inefficiencies create substantial burdens while failing to capture the adaptive behaviors characteristic of modern blockchain-based laundering.

This study addresses these limitations through three primary contributions. First, we construct *StableAML*, a large-scale, domain-specific dataset focused exclusively on stablecoin flows. We collect suspicious and malicious Ethereum wallets identified through Etherscan reports, disclosures from partner blockchain security firms (e.g., SlowMist, PeckShield), and official sanctions and enforcement lists, specifically the U.S. Office of Foreign Assets Control (OFAC) Specially Designated Nationals list. We integrate these labels with the complete transfer history of USDT and USDC on Ethereum and process the data through a feature engineering pipeline that constructs 68 domain-specific attributes organized into four distinct categories: Interaction Features, Derived Network Features, Transfer-based Features, and Temporal and Direct Features. To the best of our knowledge, this is the first study to construct a large-scale labeled dataset exclusively focused on stablecoins. This specialized scope allows us to isolate unique token mechanics, specifically smart contract freezes and blacklist interactions, that are absent in native-asset models yet critical for identifying stablecoin-specific laundering typologies. Moreover, in this emerging paradigm, the global visibility of the native chain will likely be obfuscated by privacy layers. Consequently, AML frameworks must evolve to operate within deterministic *compliance tunnels*, where decision-making is restricted to exclusive, permissioned transfer logs. This validates a methodological pivot toward models that can extract robust risk signals solely from stablecoin contract events, as these regulated liabilities will serve as the persistent, auditable “choke points” in an otherwise private ledger economy.

Second, we develop a comprehensive evaluation framework leveraging supervised machine learning to classify wallet behaviors, explicitly addressing the unique obfuscation techniques of the stablecoin ecosystem. Detecting illicit activity on-chain involves challenges distinct from traditional fraud: malicious actors rapidly dissipate illicit funds across vast wallet networks or utilize chain hopping strategies, routing funds through cross-chain bridges and decentralized exchanges, to fragment the transaction graph. Furthermore, emerging privacy technologies, specifically zero-knowledge-based shielding protocols (e.g., Railgun) and mixer services, increasingly obscure transaction linkages by cryptographically breaking the on-chain traceability between senders and recipients (Europol, 2020; Force, 2021; Manning et al., 2025). These factors create significant sparsity and structural disconnects in the transaction network, limiting the effectiveness of Graph Neural Networks (GNNs) which rely on dense, unbroken connectivity for message passing. To navigate this complexity, we compare four ensemble models against GNNs, demonstrating that ensemble methods offer improved detection capabilities. The latter prioritize intrinsic behavioral patterns over topological dependencies, which are often fragmented by these privacy mechanisms.

Third, we enhance the interpretability of AML detection to support policy and compliance efforts. Beyond predictive performance, we identify the dominant behavioral drivers underlying suspicious activity, showing which transaction patterns, service interactions, and multi-hop structures most strongly contribute to illicit classifications. This dual focus on detection and explanation allows the analysis to move beyond black-box prediction, providing actionable insights into how laundering strategies manifest on-chain and offering empirical validation for evolving financial regulations.

The remainder of the paper is organized as follows. Section 2 reviews related work on blockchain-based AML detection, privacy challenges, and regulatory enforcement. Section 3 describes the dataset construction and feature engineering process. Section 4 outlines the modeling methodology, including the evaluated machine learning and graph-based approaches. Section 5

presents the experimental results and discusses their implications, including feature importance, detected activity typologies, and binary classification analyses. Finally, Section 6 concludes the paper and highlights directions for future research.

## 2 Literature Review

Machine learning has long played an important role in fraud detection within traditional financial systems. Banks and payment networks routinely employ supervised models to identify credit card fraud and identity theft by learning patterns in user behavior, merchant characteristics, and transaction timing (Chen et al., 2018).

In this traditional context, tree ensembles have demonstrated detection capabilities comparable to deep neural networks. Recent benchmarks report F1 scores exceeding 0.90 for tabular transaction data, reinforcing their viability without the computational overhead of complex graph-based approaches (Gorte et al., 2023).

Building on this foundation, the cryptocurrency literature applies machine learning and graph analysis to identify money laundering patterns in digital assets. Shojaeinasab (2024) studies Bitcoin mixing and trains GNNs to classify links to mixers. Similarly, Pocher et al. (2023) detect illicit activity on the Bitcoin network using the Elliptic dataset to classify transactions as illicit or legitimate.

In the broader Web3 context, Lin et al. (2023) introduce the EthereumHeist dataset to analyze addresses linked to hacks and scams. Their work demonstrates that programmable obfuscation techniques, specifically token swaps and cross-chain transfers, have become central mechanisms for concealing illicit fund origins.

From a methodological perspective, Liu et al. (2023) introduce GTN2vec to identify laundering activity on Ethereum. While effective for native Ether transactions, their graph-learning approach relies on continuous transaction chains. This leaves a specific gap in addressing stablecoin ecosystems, where token mechanics often fragment the transaction graph.

Looking beyond current graph limitations, Berentsen et al. (2023) outline a future landscape where privacy-preserving technologies, specifically ZKPs, fundamentally alter the availability of public transaction data. They argue that the economic demand for privacy will drive a shift toward *selective transparency*, where transaction validity is decoupled from the public exposure of sensitive data. Manning et al. (2025) introduce the concept of *concealment enhancers*, which weaken transaction traceability. Complementing this view, Chang et al. (2020) examine blockchain adoption in financial services using qualitative evidence to highlight these monitoring challenges.

Extending the scope to stablecoins, Vatsa (2025) provides a large-scale empirical analysis highlighting strong market concentration. The authors examine how regulatory initiatives, including the EU’s MiCA and the U.S. GENIUS Act, promote transparency but may also reinforce market dominance by imposing compliance costs that act as barriers to entry. Complementing such a regulatory perspective, Griffin et al. (2025) trace illicit flows to assess the effects of interventions like OFAC sanctions and asset freezes. Their findings show that while enforcement reduces illicit mixer volume, criminal actors migrate to DeFi swaps and cross-chain bridges. Akartuna et al. (2022) argue against “one-size-fits-all” prevention strategies. They emphasize that distinct asset classes like stablecoins require tailored detection models capable of addressing their unique risk profiles and operational contexts.

Collectively, these studies show that AML strategies must integrate advanced analytical models with evolving regulatory landscapes. However, existing research remains largely focused on native cryptoassets or dependent on continuous graph topologies. This creates a critical gap for supervised, feature-centric frameworks specifically tailored to the stablecoin ecosystem,

where unique token mechanics require specialized detection strategies distinct from traditional graph-based tracing.

### 3 The *StableAML* Dataset

The Ethereum blockchain records billions of transactions. Our study narrows this scope to the value flow of the two dominant stablecoins, USDT and USDC. To isolate these movements, we query the ledger specifically for **Transfer** events emitted by the official smart contracts<sup>7</sup> between 2017–11–28 and 2025–08–08. Unlike raw transactions, which often involve complex contract interactions without actual value exchange, event logs allow us to capture definitive token movements.

Field	Value
Transaction	0xf8163c3d5ba77186ad4c6c93c4f3f92a88adb1b55cd0da34de2a44d33d4e20bd
Sender Address	0x654Fae4aa229d104CAbead47e56703f58b174bE4
Recipient Address	0x00000000035B5e5ad9019092C665357240f594e
Amount	1,092,761.61 USDT
Timestamp	2024-01-31 11:59:59

**Table 1:** Example of a real token transfer event extracted from the dataset. The transaction occurred on 2024-01-31 at 11:59:59 UTC and involved a transfer of 1,092,761.61 USDT.

Transfer events remain visible even when privacy-enhancing technologies, which obscure transaction-level details, are employed. This choice resolves ambiguities inherent in raw transaction data, particularly in meta-transaction or relayer scenarios.

For example, consider a case where a Relayer (Wallet A) submits a transaction to execute a transfer on behalf of a User (Wallet B) to a Recipient (Wallet C). The blockchain’s raw transaction ledger records Wallet A as the initiator, obscuring the true economic actor. However, the emitted **Transfer** event ignores the intermediary and correctly logs the token transfer from B to C.

By relying on these event-level records, we reconstruct value flows directly between counterparties and aggregate the observed transfers at the wallet level, constructing behavioral profiles for each address exploiting the transparency standards mandated by their technical design (Force, 2021; Europol, 2020).

Given that illicit entities constitute less than 1% of the broader Ethereum address population, we construct a statistically tractable learning dataset by selecting a representative subset of labeled wallets. This results in a curated dataset of 16,433 addresses spanning three risk categories.

#### 3.1 Classification Groups

We divide wallet addresses into three distinct classes to perform supervised learning and capture behavioral and regulatory heterogeneity within the stablecoin ecosystem:

- **Normal:** addresses with no negative flags, reflecting legitimate on-chain activity.
- **Cybercrime:** addresses identified as direct perpetrators of malicious on-chain activities. These labels are sourced from forensic reports by blockchain security firms (e.g., SlowMist,

---

<sup>7</sup>Smart contracts are self-executing programs stored on a blockchain that run when predetermined conditions are met. In the context of stablecoins, these contracts autonomously manage the issuance, transfer, and balance tracking of tokens without a centralized intermediary.

PeckShield) and community alerts. This category captures the active originators of illicit funds, including:

- Exploits & Hacks: addresses linked to DeFi protocol breaches or exchange thefts.
- Scams & Phishing: addresses associated with fraudulent schemes or social engineering attacks.
- **Blocklisted**: addresses subject to administrative interdiction or legal enforcement. Unlike the *Cybercrime* category, which is defined by active behavior, this category is defined by regulatory status and encompasses both public and private enforcement mechanisms.
  - *Sanctioned*: addresses designated by government bodies, specifically the OFAC Specially Designated Nationals (SDN). (Andersen, 2022).
  - *Frozen*: addresses blocked at the smart contract level by stablecoin issuers, rendering the assets non-transferable.

In the resulting modeling dataset, *Normal* wallets represent approximately 48.7% of observations, while *Cybercrime* and *Blocklisted* accounts comprise 36.5% and 14.8%, respectively.

## 3.2 Feature Engineering

Since money laundering on blockchains manifests through complex behavioral and relational patterns (Shojaeinasab, 2024), we construct a structured feature extraction process that quantifies wallet activity across multiple dimensions.

After assembling the engineered attributes for each wallet, we organize them in a tabular format, with each row corresponding to an address and each column representing an engineered feature (details are provided in Table 8 of Appendix A). We group the resulting 68 features into four distinct categories:

- **Interaction Features**: Describe direct wallet–protocol relationships (e.g., DeFi, Centralized Exchanges (CEX)).
- **Derived Network Features**: Track multi-hop fund propagation and indirect connections.
- **Transfer-based Features**: Characterize direct value flow and volume thresholds.
- **Temporal and Direct Features**: Capture timing patterns and intrinsic account properties.

### 3.2.1 Interaction Features

Feature construction begins by identifying the major on-chain services and protocols that wallets interact with, including swap protocols, lending platforms, and staking pools. Each represents a distinct functional layer of the Web3 ecosystem. By explicitly labeling these services and linking each transaction to the corresponding protocol, we construct features that capture how wallets route funds through intermediaries.

Table 2 summarizes three key service categories. The “Wallets” column reports the number of addresses that activate each feature. Note that the sum of these counts exceeds the total number of unique wallets, as a single address may interact with multiple service types (e.g., using both Uniswap and Aave).

Service Label	Description	Features	Wallets
Swap Protocols	Permissionless token-exchange platforms such as Uniswap or Curve.	sentToSwap, receivedFromSwap	44,312
Lending Platforms	Protocols enabling borrowing and collateralized lending, such as Aave or Compound.	sentToLending, receivedFromLending	28,904
Staking Pools	Smart contracts allowing users to lock tokens for yield or network participation.	sentToStake, receivedFromStake	12,587

**Table 2:** Service interaction labels. A wallet is counted in multiple categories if it interacts with multiple protocol types.

### 3.2.2 Derived Network Features

While interaction features capture direct relationships, derived network features capture how illicit funds propagate across the network after the initial transaction. These features track movements across multiple hops, including second- and third-degree connections to flagged wallets.

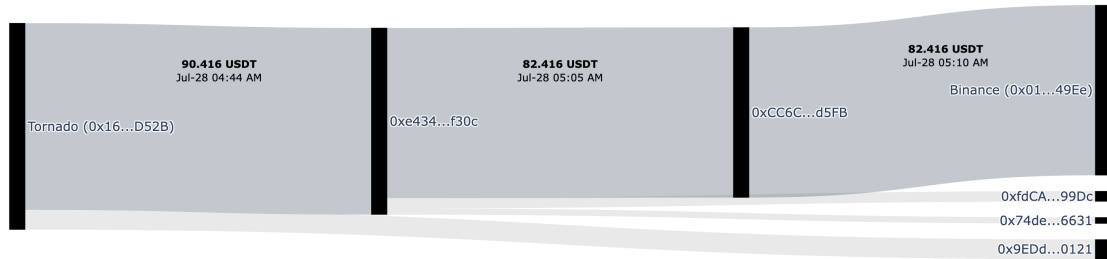


**Figure 2:** Sankey diagram of a multi-hop transfer. Funds are withdrawn from Tornado Cash, passed through intermediary wallets to obscure the trail, and rapidly deposited into a centralized exchange (Binance) within a 26-minute window. The prominent grey path highlights the primary volume flow, illustrating the "layering" behavior captured by second-degree network features.

To illustrate multi-hop exposure, Figure 2 details a real-world laundering pattern observed in the dataset. The sequence begins at 04:44 UTC with a withdrawal of approximately 90 USDT from the Tornado Cash mixer (0x16...D52B) to an intermediary wallet (0xe434...f30c). In a typical obfuscation attempt, a portion of the funds is siphoned off or paid as fees, while the bulk (82,416 USDT) is forwarded twenty minutes later to a second intermediary wallet (0xCC6C...d5FB). Finally, at 05:10 UTC, less than 30 minutes after the initial withdrawal, the funds are deposited into a Binance wallet (0x01...49e) for off-ramping<sup>8</sup>. This rapid, multi-hop transfer<sup>9</sup> during

<sup>8</sup>Off-ramping refers to the process of converting digital assets back into fiat currency or tangible goods, serving as the exit point from the blockchain ecosystem.

<sup>9</sup>Full transaction hashes: 0x5f35d27d5d17f1249f6245544f0426aeb091fdaafb16db956afa636c4ca0111d, representing the withdrawal from the Tornado Cash router to the first intermediate wallet; 0x41c2e200e8d078883f88aceaf117acb9230a25e7ddce46378f4128e50b74abf1, recording the transfer from the first intermediate wallet to a downstream recipient approximately twenty minutes after the mixer withdrawal; and 0x4a5be4a5df2099cc53eedaba8b9185c465d0d8dc55591475d971cf1ea46fcca, representing the subsequent transfer from the downstream wallet to the final destination address.

off-peak hours exemplifies the structural "hop" patterns our derived features are engineered to detect.

To appreciate the role of interaction and derived network features, Figure 3 visualizes the distribution of key indicators. The left panel demonstrates the structural difference in indirect risk exposure: while legitimate users have zero exposure to high-value laundering flows, Blocklisted and Cybercrime wallets show a distinct distribution of second-degree connections to transfers exceeding \$10k (`2ndWithOver10k`). The right panel highlights the operational divergence: legitimate users favor Centralized Exchanges (`sentToCex`), whereas illicit actors predominantly route funds through decentralized swap protocols.

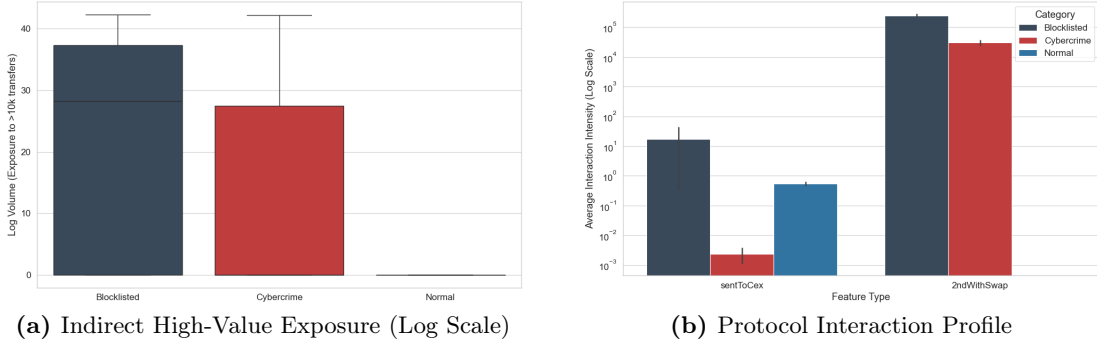


**Figure 3:** Exploratory plots. (a) Distribution of `2ndWithOver10k` shows that illicit wallets are structurally embedded in high-volume networks, unlike normal users. (b) Inverse preference for CEX vs. DeFi Swaps.

### 3.2.3 Transfer-based Features

Transfer-based features capture the direct flow of value *into* and *out* of a wallet. These include threshold-based indicators, such as transfers exceeding \$1,000, \$5,000, and \$10,000. Their design draws on the classic AML literature, which notes that illicit funds typically move through identifiable entry and exit channels during the placement and integration stages of laundering. Rather than assuming these stages *a priori*, the features capture transactional patterns consistent with them, allowing the model to learn whether such movements signal elevated risk.

### 3.2.4 Temporal and Direct Features

Temporal behavioral features track time-based patterns such as daily transfer bursts, repeated identical-value movements, and rapid reciprocals. These highlight abnormal rhythms often aligning with laundering practices, such as sudden high-frequency inflows. To illustrate, the address `0x03d09ec664f9241b23223240a06079300de1b14d` sends a sequence of repeated 50,000 USDT transfers to the recipient `0xeFd2fd5c18093030E15a08fF8799BEC9c612Ec4f`. On 2025-08-08, the recipient receives four such transfers in less than fifteen minutes, totaling 200,000 USDT. Table 3 provides a concrete example of the temporal anomalies these features are designed to capture.

Transaction	Timestamp	USDT
0xeb073c65c481114289e8aa63d86ca36ae79854eb270b58ce12961c4d41666124	2025-08-08 03:04:47 UTC	50,000
0x16a3e2bb4c73bc50324b3ba24ae391ae3ead13e90deed2ea835f3c1fb4e780cb	2025-08-08 03:04:59 UTC	50,000
0x74b8321b5c8817e0dc00c21907e8a85673f1762caa21a3d52328ca6421db6e59	2025-08-08 03:20:11 UTC	50,000
0xb4a930b2e5aaf8d09055fea6eda1a134cb1524ba6be86418119eb1714d4329a1	2025-08-08 03:20:23 UTC	50,000

**Table 3:** Temporal excerpt showing repeated identical-value inflows of 50,000 USDT from `0x03...` to `0xeF...`

Finally, direct features capture intrinsic properties of a wallet that do not depend on interactions with other addresses. These include whether the address is an externally owned account (EOA)<sup>10</sup>, whether its contract code is verified<sup>11</sup>, and indicators of prolonged activity<sup>12</sup>. These properties help distinguish ordinary user wallets from ephemeral or synthetic addresses frequently observed in laundering operations.

### 3.3 Graph Construction

While the feature-based classifiers described previously excel at identifying individual suspicious behaviors, they treat each wallet as an independent entity, potentially overlooking the complex, collaborative nature of money laundering networks. To bridge this gap, we complement the tabular analysis with a graph approach, explicitly modeling the transaction ecosystem to capture how illicit flows propagate between accounts.

To leverage the relational structure of the ecosystem, we model the data as a weighted directed graph  $\mathcal{G} = (\mathcal{V}, \mathcal{E})$ .

- **Nodes ( $\mathcal{V}$ ):** The set of unique wallet addresses identified in the *StableAML* dataset.
- **Edges ( $\mathcal{E}$ ):** For each ordered pair of wallets  $(A, B)$  with at least one observed transfer, we define a directed edge  $e_{A \rightarrow B}$ . The edge weight  $w_{A \rightarrow B}$  equals the total stablecoin volume transferred from  $A$  to  $B$ , aggregated over the full temporal span of the dataset.

We formulate the detection task as supervised multiclass node classification, mapping each node  $v$  to a risk category  $y \in \{Normal, Cybercrime, Blocklisted\}$ . To integrate behavioral insights, we initialize each node  $v \in \mathcal{V}$  with a feature vector  $\mathbf{x}_v \in \mathbb{R}^{68}$ , corresponding to the engineered attributes defined in Section 3.2.

Consistent with the tabular setting, we construct the graph over the curated set of labeled wallets and perform a wallet-level train–test split on this fully labeled node set, as explained in the following section. The splits are disjoint, ensuring that no wallet appears in both training and test sets. As both the graph structure and node features are cumulative aggregates over the full observation window, the task is formulated as static multiclass node classification.

<sup>10</sup>An EOA refers to a standard user-controlled wallet managed by a private key, in contrast to a smart contract account whose behavior is defined by on-chain code.

<sup>11</sup>A verified smart contract publishes its source code and metadata on block explorers such as Etherscan, enabling public inspection and confirmation that the deployed bytecode matches the published source.

<sup>12</sup>Prolonged activity refers to wallets that remain active over extended periods, as opposed to short-lived or disposable addresses often used in obfuscation or layering schemes.

## 4 Modeling Methodology

In this section, we formalize the multiclass wallet classification task and outline the evaluation framework. The task is a three-class classification problem ( $K = 3$ ), labeling wallets that transfer USDT or USDC according to the categories defined in Section 3. Additionally, we provide results for a binary classification setup ( $K = 2$ ) to further analyze the models’ efficacy in distinguishing between broader risk categories.

Given the strong class imbalance, with *Cybercrime* and *Blocklisted* wallets comprising a small fraction of the raw ecosystem, we evaluate all models using the Macro-F1 Score ( $F1_{\text{Macro}}$ ). This metric treats each class equally and emphasizes the balance between precision and recall, which is more informative than overall accuracy under label imbalance. While we also report the *Area Under the Receiver Operating Characteristic* (AUROC) for completeness, it is considered a secondary metric here, as AUROC tends to yield overly optimistic results in the presence of highly skewed class distributions. In AML settings, this balance is critical: false negatives carry substantially higher regulatory and operational costs than false positives. Missing an illicit wallet can enable the continuation of criminal flows, expose institutions to sanctions, and violate compliance obligations, as highlighted by the Financial Action Task Force risk-based framework (Force, 2021). Prior AML research similarly argues that recall deserves particular attention when the goal is to identify rare but high-risk entities (Shojaeinasab, 2024).

We split the dataset into training and test sets using an 80/20 partition, resulting in 13,146 training samples and 3,287 independent test samples. The test portion serves as a fully isolated holdout set for the final assessment of generalization performance.

The resulting class distribution within these partitions allows the model to learn detailed risk patterns that would otherwise be statistically overwhelmed by the majority class, without relying on synthetic data generation. After selecting the best configuration, we retrain the model on the full training split and evaluate it once on the holdout test set. The complete set of optimized hyperparameters for all models appears in Appendix B.

### 4.1 Logistic Regression

We use logistic regression (LR) as an interpretable baseline to assess the discriminatory power of the engineered features under linear decision boundaries. We adopt the multinomial logistic regression formulation, which generalizes logistic regression to multiclass problems by modeling the joint probability distribution across all  $K$  classes simultaneously.

The predicted probability that a wallet with feature vector  $\mathbf{x} \in \mathbb{R}^{68}$  belongs to class  $k$  is computed using the softmax function:

$$P_k(\mathbf{x}) = \frac{\exp(\beta_k^\top \mathbf{x} + \beta_{0,k})}{\sum_{j=1}^K \exp(\beta_j^\top \mathbf{x} + \beta_{0,j})}, \quad k \in \{0, 1, 2\}$$

where  $\beta_k \in \mathbb{R}^{68}$  denotes the class-specific coefficient vector,  $\beta_{0,k}$  represents the intercept for class  $k$ , and  $K = 3$  corresponds to the total number of risk categories. The final class assignment is determined by selecting the category with the highest probability mass:

$$\hat{y}(\mathbf{x}) = \underset{k}{\operatorname{argmax}} P_k(\mathbf{x})$$

Model parameters are estimated by minimizing the categorical cross-entropy loss. We utilize the SAGA solver to optimize the objective function, as it provides efficient convergence for datasets with high-dimensional feature spaces and supports the  $L_1$  regularization penalties explored in our grid search.

## 4.2 Tree Ensembles

Ensemble learning aggregates predictions from multiple base estimators to improve generalization and robustness compared to a single model. We leverage this paradigm to capture the complex, non-linear feature interactions characteristic of money laundering patterns. Specifically, we benchmark four tree ensembles selected for their proven efficacy in handling heterogeneous behavioral signals and sparse transaction data (Chen et al., 2018; Shojaeinasab, 2024): Random Forest (RF) and three Gradient Boosting Machines (GBMs): XGBoost, LightGBM, and CatBoost.

RF employs bagging to reduce variance by aggregating predictions from an ensemble of independent decision trees. The predicted probability that a wallet with features  $\mathbf{x}$  belongs to class  $k$  is computed as the average of the empirical class proportions produced by each of the  $M$  individual trees, where  $P_m(y = k | \mathbf{x})$  denotes the fraction of training samples of class  $k$  in the terminal leaf of tree  $m$ . To optimize the decision nodes, we employ the Gini impurity index as the splitting criterion, and the final class assignment follows:

$$\hat{y}(\mathbf{x}) = \underset{k}{\operatorname{argmax}} P_k(\mathbf{x}).$$

In contrast to the independent training of RF, GBMs construct an additive model in a forward stage-wise fashion. They iteratively fit new decision trees to the negative gradient of the loss function associated with the current ensemble’s prediction, effectively performing gradient descent in function space to minimize a global objective.

To address the multiclass nature of our task, we adopt the native multiclass formulation implemented in XGBoost, LightGBM, and CatBoost. In this setting, the ensemble produces a vector of class-specific scores (logits)  $F_k(\mathbf{x})$ , obtained by aggregating the contributions of  $M$  trees:

$$F_k(\mathbf{x}) = \sum_{m=1}^M f_{m,k}(\mathbf{x}).$$

The class probabilities are computed using the softmax function:

$$P_k(\mathbf{x}) = \frac{\exp(F_k(\mathbf{x}))}{\sum_{j=1}^K \exp(F_j(\mathbf{x}))},$$

and the predicted label is given by

$$\hat{y}(\mathbf{x}) = \underset{k}{\operatorname{argmax}} P_k(\mathbf{x}).$$

Model parameters are optimized by minimizing the multinomial cross-entropy loss:

$$\mathcal{L} = -\frac{1}{n} \sum_{i=1}^n \sum_{k=1}^K y_{i,k} \log P_k(\mathbf{x}_i).$$

The complete configuration of grid search spaces and optimal hyperparameters is detailed in Appendix B.

## 4.3 Deep Neural Network

To capture high-order non-linear feature interactions, we implement a Deep Neural Network (DNN) architecture consisting of two fully connected hidden layers. Non-linearity is induced via Rectified Linear Unit (ReLU) activations, defined as  $f(x) = \max(0, x)$ . To improve generalization and

prevent overfitting on the high-dimensional feature space, we incorporate dropout regularization, which randomly masks a fraction of neuronal connections during the training phase.

The final hidden representation is linearly projected to a vector of unnormalized logits  $\mathbf{z} \in \mathbb{R}^K$  and normalized using the softmax function:

$$P_k(\mathbf{x}) = \frac{\exp(z_k(\mathbf{x}))}{\sum_{j=1}^K \exp(z_j(\mathbf{x}))}. \quad (1)$$

The predicted class label  $\hat{y}$  is determined by selecting the category with the highest probability mass, as follows:

$$\hat{y}(\mathbf{x}) = \operatorname{argmax}_k P_k(\mathbf{x}).$$

Model parameters are optimized using the Adam algorithm by minimizing the categorical cross-entropy loss over the  $n$  training samples:

$$\mathcal{L} = -\frac{1}{n} \sum_{i=1}^n \sum_{k=1}^K y_{i,k} \log P_k(\mathbf{x}_i),$$

where  $y_{i,k} \in \{0, 1\}$  is the binary indicator for the true class membership of sample  $i$ , and  $P_k(\mathbf{x}_i)$  denotes the predicted class probability.

#### 4.4 Graph Neural Network Architecture

We adopt the GraphSAGE architecture Hamilton et al. (2017), which learns neighborhood aggregation functions rather than node-specific embeddings. While our experiments are conducted on a curated labeled subgraph with a wallet-level train–test split, the inductive design allows the model to generalize by aggregating local neighborhood features, making it well-suited for large and evolving transaction networks.

The architecture consists of two spatial convolution layers equipped with neighbor sampling to handle graph sparsity. At layer  $l$ , the model updates the representation of node  $v$  by concatenating its current embedding with an aggregated summary of its local neighborhood. We utilize the mean aggregator for its efficiency and permutation invariance. The update rule is formally defined as:

$$h_v^{(l)} = \sigma \left( W^{(l)} \cdot \left[ h_v^{(l-1)} \parallel \frac{1}{|\mathcal{N}(v)|} \sum_{u \in \mathcal{N}(v)} h_u^{(l-1)} \right] \right),$$

where  $h_v^{(0)} = \mathbf{x}_v$  corresponds to the initial feature vector described in Section 3.2,  $\parallel$  denotes the concatenation operation, and  $W^{(l)}$  is a learnable weight matrix. The term within the summation computes the element-wise mean of the neighbor embeddings, capturing the average behavioral profile of a wallet’s direct transactors.  $\sigma$  represents the non-linear activation function (typically a Rectified Linear Unit (ReLU)).

After  $L = 2$  layers of aggregation, the final node embeddings  $h_v^{(L)}$  are projected to the output space corresponding to the three target classes via a linear transformation. The class probabilities are obtained by applying the softmax function:

$$P_k(h_v^{(L)}) = \frac{\exp(z_{v,k})}{\sum_{j=1}^K \exp(z_{v,j})},$$

The predicted label is then given by  $\hat{y}_v = \operatorname{argmax}_k P_k(h_v^{(L)})$ .

## 5 Results and Discussion

This section presents the empirical findings of the proposed framework and discusses their implications for detecting suspicious activity in stablecoin ecosystems. We first evaluate model performance in the full three-class setting. We then examine feature importance to identify which behavioral and relational attributes most strongly influence predictive performance. Building on these results, the following subsection analyzes how these features align with known suspicious activity typologies, revealing structural differences between illicit and restricted wallet behaviors. We further interpret the detected patterns, linking them to characteristic money-laundering mechanisms and transaction-flow signatures. Finally, for comparability with prior work, we evaluate a simplified binary classification setup that collapses all suspicious wallets into a single class, providing an additional perspective on the expressiveness and robustness of the engineered feature space.

To facilitate reproducibility, the StableAML Dataset used in this study is available at <https://github.com/finos-labs/dtcch-2025-OpenAML> (OpenAML Project under the Linux Foundation FINOS initiative).

### 5.1 Per-Class Performance Analysis

We begin by examining the detailed breakdown of classification performance across the three target classes: *Normal*, *Cybercrime*, and *Blocklisted*. Table 4 presents the precision, recall, F1-score, and OvR AUROC for each category.

A critical observation concerns the divergence between AUROC and F1-score, particularly for the linear baseline. While LR achieves AUROC values above 0.93 for all classes, its recall for the *Blocklisted* class drops to 0.49. This confirms that AUROC can be overly optimistic in imbalanced settings, masking significant false negatives. Consequently, we prioritize the F1-score and Recall as the primary indicators of operational utility.

The results reveal clear distinctions in learnability across risk typologies:

- **Normal & Cybercrime:** Tree ensembles achieve near-optimal performance for these categories, with F1-score exceeding 0.98. This indicates that the engineered behavioral features effectively capture the consistent and often automated transaction patterns associated with both legitimate high-frequency users and professionalized cybercrime operations.
- **Blocklisted:** Classification of this category proves substantially more challenging. Although ensemble methods significantly outperform the LR baseline ( $F1 \approx 0.95$  vs. 0.63), the gap between precision and recall is most pronounced here. This difficulty reflects the heterogeneous nature of the Blocklisted class, which includes wallets frozen for diverse reasons, from sanctions evasion to theft recovery, resulting in less uniform transactional footprints than the active Cybercrime wallets.

Deep learning approaches (DNN and GNN) exhibit marked instability in this minority class. The GNN, in particular, struggles to recall Blocklisted entities ( $Recall \approx 0.74$ ), lagging behind CatBoost ( $Recall \approx 0.95$ ) by a wide margin. This suggests that in the absence of a dense transaction graph, deep learning models fail to recover the subtle signals that tree ensembles successfully extract from the tabular features.

Model	Class	AUROC	Precision	Recall	F1
Logistic Regression	Normal	0.9453	0.7877	0.9988	0.8807
	Cybercrime	0.9351	0.9375	0.7614	0.8403
	Blocklisted	0.9353	0.8773	0.4896	0.6285
CatBoost (Best)	Normal	0.9990	0.9927	1.0000	0.9963
	Cybercrime	0.9991	0.9873	0.9831	0.9852
	Blocklisted	0.9943	0.9579	0.9440	0.9509
GNN	Normal	0.9735	0.7725	0.9601	0.8557
	Cybercrime	0.9647	0.9010	0.7366	0.8109
	Blocklisted	0.9667	0.9592	0.6131	0.7481

**Table 4:** Detailed per-class performance metrics on the test set. Note the significant drop in Recall for the Blocklisted class in non-ensemble models, despite high AUROC values.

The complete performance breakdown, demonstrating consistent high efficacy across different models, is detailed in Appendix Table 12.

## 5.2 Overall Model Comparison

Aggregating performance across all categories, Table 5 summarizes the macro-averaged metrics for the evaluated models. The results demonstrate a clear hierarchy of model efficacy, with tree ensembles substantially outperforming both linear baselines and deep learning approaches.

Model	AUROC	Accuracy	F1	Recall
Logistic Regression	0.9385	0.8387	0.7831	0.7499
Random Forest	0.9976	0.9824	0.9714	0.9708
LightGBM	0.9976	0.9845	0.9755	0.9742
<b>CatBoost</b>	<b>0.9974</b>	<b>0.9857</b>	<b>0.9775</b>	<b>0.9757</b>
XGBoost	0.9974	0.9851	0.9766	0.9760
DNN	0.9617	0.9192	0.8708	0.8504
GNN	0.9683	0.8290	0.8048	0.7699

**Table 5:** Overall multiclass classification performance (macro-averaged metrics). CatBoost demonstrates the best balance between precision and recall across all risk categories.

GBMs consistently achieve strong discrimination across all evaluation metrics, with average AUROC values exceeding 0.997 and Macro-F1 scores ranging between 0.975 and 0.979. Performance is robust and well-balanced: the *Normal* class exhibits near-perfect precision and recall, the *Cybercrime* class is identified with F1 scores of approximately 0.98, and even the heterogeneous *Blocklisted* class achieves F1 scores of approximately 0.95.

These results highlight the adaptability of tree ensembles to the specific properties of blockchain transaction data. As noted in broader machine learning literature, they frequently outperform deep neural networks on tabular datasets dominated by binary or dummy-encoded indicators, as they naturally partition the feature space along discrete signals without the need for extensive smoothing or manifold learning (Grinsztajn et al., 2022). Our engineered feature set contains many such behavioral flags (e.g., `isVerifiedContract`, `hasProxyBehaviour`), which these ensembles exploit effectively to isolate high-risk typologies.

In contrast, the deep learning approaches perform less competitively. While both DNN and GNN models achieve AUROC values above 0.96, their Macro-F1 scores plateau around 0.80–0.87.

A central finding is the underperformance of the GraphSAGE, which fails to improve upon the DNN baseline ( $F1 \approx 0.805$  vs  $0.871$ ).

This outcome reflects data constraints specific to the stablecoin ecosystem. The resulting transaction graph exhibits extreme sparsity (density  $< 0.01$ , where density denotes the fraction of observed edges relative to the maximum number of possible directed edges  $|\mathcal{V}|(|\mathcal{V}| - 1)$ , excluding self-loops), primarily because the analysis is intentionally restricted to USDT and USDC transfers. Money laundering workflows frequently involve rapid swaps of stablecoins into volatile assets (e.g., ETH, WBTC) via decentralized exchanges to break the transaction chain. Since these intermediate cross-asset interactions are excluded from a stablecoin-only graph, the connectivity required for effective message passing is broken. Consequently, the GNN cannot capture the multi-hop layering patterns that are otherwise visible to the ensemble models via engineered aggregate features (e.g., `2ndWithSwap`).

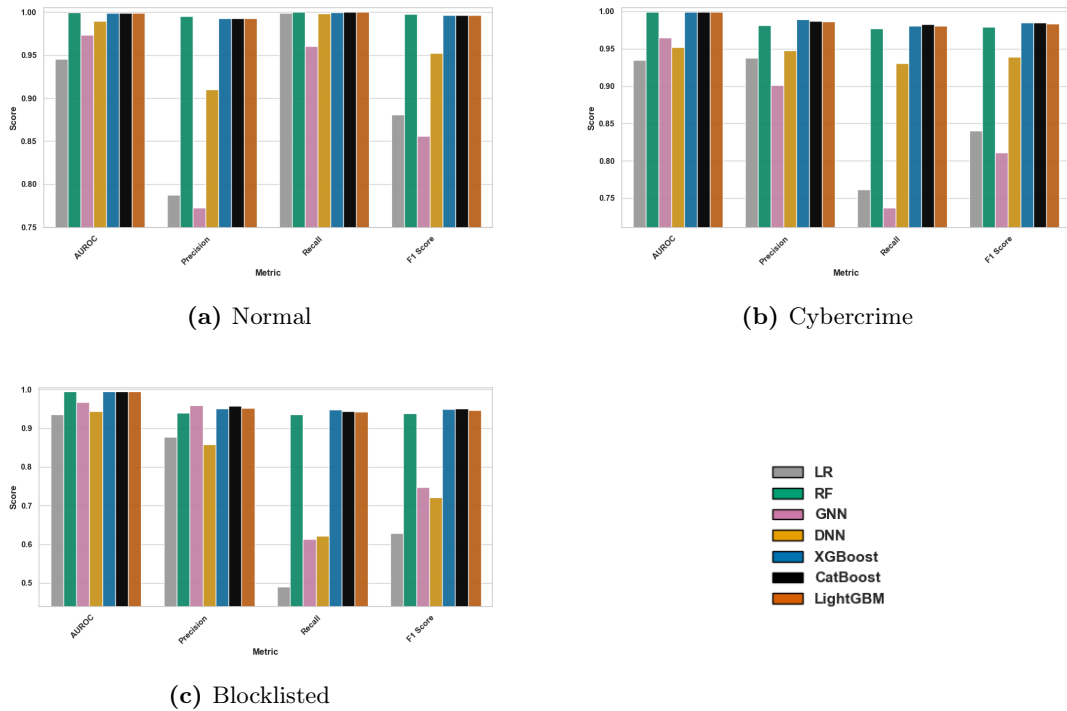


**Figure 4:** Per-class OvR performance curves for multiclass wallet classification, shown separately for the *Normal*, *Cybercrime*, and *Blocklisted* classes.

The detailed per-class performance analysis, summarized in Figure 4, reveals clear architectural differences in how models handle distinct risk typologies. For the *Normal* and *Cybercrime* classes (Panels (a) and (b)), all tree ensembles achieve near-optimal performance, with precision and recall closely aligned across models. This result indicates that the engineered behavioral features effectively capture the consistent and often automated transaction patterns associated with large-scale cybercrime and hacking activity.

In contrast, classification performance for the *Blocklisted* class (Panel (c)) remains substantially more challenging. Although ensemble methods continue to outperform the linear baseline, with F1 improvements exceeding 0.13, this category exhibits the highest variance in detection rates.

This reflects the heterogeneous nature of restricted wallet behavior, arising from post-enforcement dynamics rather than uniform illicit activity. Notably, the DNN and GNN models exhibit significant instability in this setting, particularly in recall, underscoring their sensitivity to sparse relational structures. This reinforces our conclusion that tree ensembles provide the most robust balance between precision and recall for detecting rare, heterogeneous risk events.

### 5.3 Feature Importance

To ensure the robustness of our findings and avoid the biases inherent in any single interpretability method, we implement a multi-stage Consensus Ranking pipeline. This approach identifies the most stable predictors of illicit activity by aggregating signals from three complementary importance measures:

1. **Model-Specific Importance (Built-in):** We extract the native importance scores from each model. For tree ensembles, this corresponds to *Gini Importance* or *Mean Information Gain*, measuring how much each feature contributes to reducing node impurity across all trees. For LR, we utilize the absolute values of the normalized coefficients ( $\beta$ ).
2. **Model-Agnostic Permutation Importance:** To assess the functional impact of features on unseen data, we perform permutation importance on the full holdout test set. This method calculates the drop in the model’s *Macro-F1 score* when feature values are randomly shuffled, effectively measuring the model’s dependence on that specific signal. We conducted 10 shuffling repetitions per feature.
3. **SHAP Values:** For the ensemble models, we compute SHAP<sup>13</sup> values using the **TreeExplainer** framework to capture complex non-linear interactions. Due to the high computational cost of the Shapley value estimation, we utilized a representative subsample of 3,000 observations from the test set to bound memory requirements while maintaining a confidence interval for the importance estimates.

For each model–importance method pair, features were sorted in descending order of importance and assigned ordinal ranks (1 = most important). For each feature, we computed the simple average of its ranks across all models and methods. Finally, features were re-ranked based on this average to obtain the Consensus Rank.

---

<sup>13</sup>SHAP library available at <https://github.com/shap>

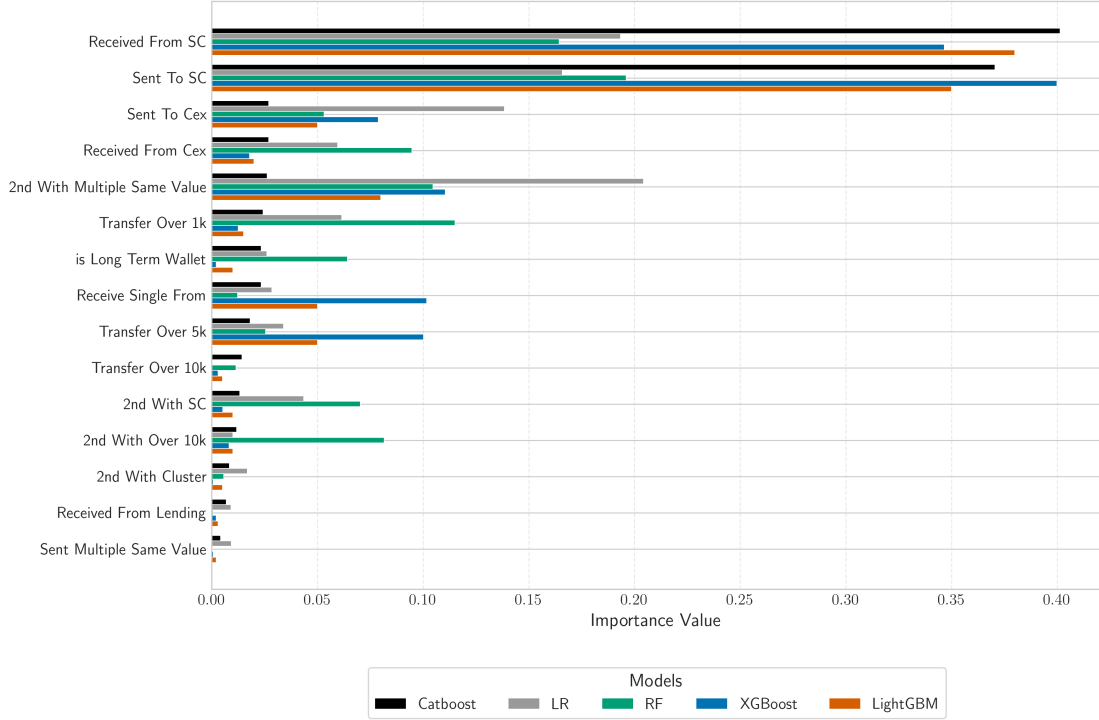


**Figure 5:** Consensus ranking of the top 15 features across primary models. The reported "Value" represents the normalized importance derived from the multi-stage pipeline, aggregating: (i) model-specific impurity/gain for tree ensembles, (ii) normalized coefficients ( $\beta$ ) for LR, (iii) model-agnostic permutation importance on the test set, and (iv) SHAP values. This rank-based aggregation ensures that the hierarchy reflects a stable consensus across both linear and non-linear estimators.

The results, consolidated across all models evaluated, show a clear prioritization of structural and volumetric indicators. The most influential features involve direct interactions with smart contracts (`receivedFromSC`, `sentToSC`) and volume thresholds, specifically `transferOver1k` and `transferOver5k`, which act as immediate behavioral discriminators. Furthermore, the high ranking of second-degree exposure features, such as `2ndWithMultipleSameValue` (exposure to wallets performing repeated identical-value transfers) and `2ndWithOver10k` (indirect connections to high-value flows), underscores the models' ability to look beyond immediate neighbors and identify the structural "hop" patterns characteristic of layering stages in money laundering.

## 5.4 Class-Specific Behavioral Signatures

To examine how predictive signals differ across wallet categories, we analyze feature importance segmented by output class. Figure 6 presents a heatmap where color intensity reflects the relative influence of each feature on class-specific predictions.

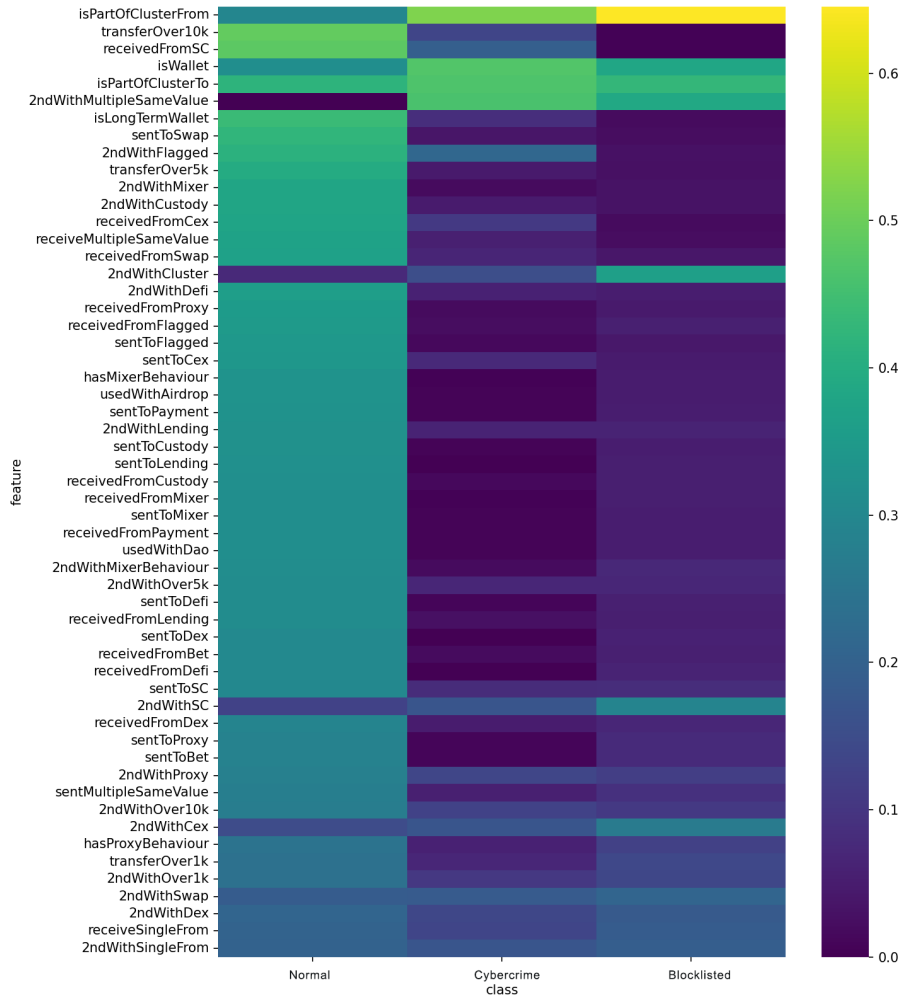


**Figure 6:** Class-specific feature importance heatmap. Color intensity represents the relative influence (normalized aggregated importance) of each feature on model predictions, segmented by output class. Values are averaged across all tree ensembles to highlight the distinct behavioral signatures of classes.

The analysis reveals a clear behavioral separation between the risk categories. Comparing across the classes (horizontally), we observe substantial consistency: features predictive for the *Normal* class generally retain relevance for the *Blocklisted* class, and vice versa. However, a vertical comparison of the features within each class reveals distinct behavioral profiles that align with classical money laundering stages (Lin et al., 2023):

1. **Normal:** As expected, this class exhibits uniformly low feature importance across the illicit-specific indicators. The model distinguishes benign activity by the absence of the strong, coordinated signals present in the suspicious categories, providing a data-driven justification for our three-class framework.
2. **Cybercrime:** This class is characterized by complex network features, including cluster membership derivatives (`isPartOfClusterFrom`, `isPartOfClusterTo`) and indirect rela-

tional exposure (`2ndWithMultipleSameValue`). This deep, structured signal is consistent with the automated *layering* stage. Professionalized groups route funds through numerous intermediary wallets to obscure origins, often responding to enforcement by increasing transaction hops and shifting to decentralized bridges (Griffin et al., 2025).

3. **Blocklisted:** In contrast, this class displays a concentrated reliance on direct interactions (`sentToSC`, `receivedFromCex`) and simpler network connections. This suggests behavior less driven by complex layering and more reflective of *placement* or constrained post-enforcement activity. As noted in (Griffin et al., 2025), sanctioned wallets typically exhibit reduced mobility and simpler transactional paths, often attempting reactive reallocations to non-freezable tokens like DAI.

Feature Group	AML Stage	Observed Behavioral Pattern
SC & CEX Flows	Placement	Direct interaction with smart contracts and centralized endpoints for initial fund entry.
Clustering & Hops	Layering	High relevance of <code>2ndWithMultipleSameValue</code> and multi-hop flows for obfuscation.
Long-Term Retention	Integration	Use of <code>isLongTermWallet</code> and large-value transfers to identify re-integration points.

**Table 6:** Principal features mapped to money-laundering typologies.

Beyond predictive performance, these results show that the models recover patterns closely aligned with the classical stages of money laundering:

- **Placement:** Funds enter via CEXs or initial SC interactions (`receivedFromCex`, `sentToSC`), where mixers often weaken the direct link to the origin (Lin et al., 2023).
- **Layering:** Obfuscation is captured by `transferOver1k/5k/10k` and `2ndWithMultipleSameValue`, reflecting value fragmentation and proxy behavior through pass-through wallets (Lin et al., 2023). These signals align with the use of cross-chain bridges and DEXs that lack KYC to facilitate asset swaps.
- **Integration:** Re-integration is indicated by `isLongTermWallet`, identifying wallets that retain funds before redistribution, and continued mixer interactions for re-anonymization (Pocher et al., 2023)

To identify the limitations of the proposed framework, we conducted a qualitative analysis of the instances where the best-performing model (CatBoost) produced errors. The primary source of False Positives stems from legitimate high-frequency traders and arbitrage bots. These actors exhibit rapid, high-volume capital flows through centralized exchanges (CEXs) and DeFi protocols, behavioral signatures that structurally mimic the *Placement* and *Layering* stages of money laundering. In the multiclass setting, residual confusion arises between the *Cybercrime* and *Blocklisted* categories. Since both groups operate under adversarial constraints, they frequently employ overlapping obfuscation mechanisms (e.g., CEX pass-throughs and rapid swaps) prior to specific enforcement actions, creating a degree of transactional ambiguity that challenges even non-linear decision boundaries.

## 5.5 Binary Classification Results

To benchmark the proposed framework against established baselines in the literature, we evaluate a simplified binary classification setting (Normal vs. Suspicious). In this formulation, the *Cybercrime* and *Blocklisted* classes are merged into a single *Suspicious* category.

To provide context, we compare our results with methods applied to the Elliptic dataset (Pocher et al., 2023), the standard benchmark for illicit activity detection in Bitcoin. It is important to note the structural differences: while the Elliptic dataset models the Bitcoin graph, our work focuses on the Ethereum account-based model restricted to stablecoin flows. Despite these differences, both tasks share the fundamental objective of separating licit from illicit entities within high-noise transaction networks, making the comparison of methodological effectiveness relevant.

Under this reduced task, the models achieve near-perfect discrimination, confirming the strong expressiveness of the engineered feature set when the problem is simplified to separating benign from suspicious behavior. As reported in Table 7, the best-performing tree ensemble model attains an F1 score of 0.999, substantially exceeding benchmarks reported in earlier work on graph-based detection. For example, studies based on the Elliptic dataset (Pocher et al., 2023) document persistent trade-offs between precision and recall, even for advanced subgraph-based classifiers such as RevClassify, a subgraph-based deep learning model designed to mine local structural patterns to overcome label scarcity. The superior performance observed here suggests that for account-based stablecoin networks, domain-specific feature engineering (e.g., second-degree exposure and cluster derivatives) offers a marked advantage over purely topological subgraph mining.

Model	AUROC	Accuracy	F1-Score	Recall
GCN (Elliptic1)	–	0.8440	0.9730	–
GAT (Elliptic1)	–	0.7230	0.9710	–
Random Forest (Elliptic1)	–	0.7820	0.9770	–
RevClassifyDS (Elliptic2)	0.9740	–	0.9530	–
Logistic Regression	0.9997	0.9953	0.9918	0.9959
Random Forest	1.0000	0.9997	0.9994	0.9988
CatBoost	1.0000	0.9995	0.9991	1.0000
LightGBM	1.0000	0.9998	0.9997	1.0000
XGBoost	1.0000	0.9993	0.9988	0.9994
DNN	0.9994	0.9998	0.9997	0.9994
GNN	0.9974	0.9929	0.9886	0.9897

**Table 7:** Binary classification performance (Normal vs. Suspicious) comparing prior benchmark results from the Elliptic dataset with models evaluated in this study.

By successfully mapping algorithmic importance to established financial crime typologies, the framework demonstrates that domain-informed feature engineering provides a robust foundation for explainable AML detection, bridging the gap between machine learning performance and regulatory interpretability.

## 6 Conclusion

The evolution of blockchain privacy presents a diverging path for compliance. While decentralized protocols increasingly adopt ZKPs to obfuscate transaction graphs, centralized stablecoins like

USDT and USDC face a different reality: to maintain fiat convertibility and acceptance by regulated entities, they must guarantee auditable provenance. This creates a persistent reliance on transparent ledger histories, not merely as a technical feature, but as a prerequisite for verifying legitimate origin in an increasingly scrutinized ecosystem.

As the industry shifts from probabilistic risk assessment toward deterministic verification, where users must mathematically prove that funds are free from contact with blocklisted addresses, stablecoins will remain the critical "transparent choke points" of the crypto economy. This study demonstrates that analyzing only these transparent footprints allows for the reliable detection of illicit actors, even as they attempt to exit through privacy-preserving protocols.

Our benchmarking revealed that domain-informed feature engineering is the decisive factor in this setting. Tree ensembles consistently outperformed deep learning approaches, achieving Macro-F1 scores above 0.97 by effectively partitioning the feature space along discrete behavioral signals. We also successfully dissect distinct typologies, differentiating the complex, multi-hop layering of *Cybercrime* syndicates from the constrained movements of *Blocklisted* entities.

By mapping these algorithmic predictions to established financial crime stages, placement, layering, and integration, we provide a scalable methodology that anticipates the future of AML: a framework robust enough to operate where transparency is mandatory, serving as a durable line of defense in a hybrid financial landscape.

## References

- Akartuna, E. A., Johnson, S. D., and Thornton, A. (2022). Preventing the money laundering and terrorist financing risks of emerging technologies: An international policy delphi study. *Technological Forecasting and Social Change*, 179:121632.
- Andersen, R. (2022). Sanctioned addresses and blockchain monitoring. Office of Foreign Assets Control (OFAC).
- Berentsen, A., Lenheimer, J., and Schär, F. (2023). An introduction to zero-knowledge proofs in blockchains and economics. *Federal Reserve Bank of St. Louis Review*, 105(4):268–283.
- Chang, V., Baudier, P., Zhang, H., Xu, Q., Zhang, J., and Arami, M. (2020). How blockchain can impact financial services – the overview, challenges and recommendations from expert interviewees. *Technological Forecasting and Social Change*, 158:120166.
- Chen, Z., Van Khoa, L. D., Teoh, E. N., Nazir, A., Karuppiah, E. K., and Lam, K. S. (2018). Machine learning techniques for anti-money laundering (aml) solutions in suspicious transaction detection: a review. *Knowledge and Information Systems*, 57(2):245–285.
- Clark, J., Demirag, D., and Moosavi, M. (2019). Sok: demystifying stablecoins. *Communications of the ACM*, Forthcoming.
- Europol, E. (2020). Internet organised crime threat assessment.
- Force, F. A. T. (2021). *Updated guidance for a risk-based approach to virtual assets and virtual asset service providers*. FATF.
- Gorte, A. S., Mohod, S. W., Keole, R. R., Mahore, T. R., and Pande, S. (2023). Credit card fraud detection using various machine learning and deep learning approaches. In Gupta, D., Khanna, A., Hassaniien, A. E., Anand, S., and Jaiswal, A., editors, *International Conference on Innovative Computing and Communications*, volume 492 of *Lecture Notes in Networks and Systems*, pages 621–628. Springer Nature Singapore, Singapore.

- Griffin, J. M., Mei, K., and Wang, Z. (2025). Are crypto anti-money laundering policies effective? *SSRN Electronic Journal*, pages 1–60. Available at SSRN: <https://ssrn.com/abstract=5522378>.
- Grinsztajn, L., Oyallon, E., and Varoquaux, G. (2022). Why do tree-based models still outperform deep learning on tabular data? In *Thirty-sixth Conference on Neural Information Processing Systems Datasets and Benchmarks Track*.
- Hamilton, W., Ying, Z., and Leskovec, J. (2017). Inductive representation learning on large graphs. *Advances in neural information processing systems*, 30.
- Lin, D., Wu, J., Fu, Q., Yu, Y., Lin, K., Zheng, Z., and Yang, S. (2023). Towards understanding crypto money laundering in web3 through the lenses of ethereum heists. In *Proceedings of the ACM SIGMETRICS Conference*, pages 1–21.
- Liu, J., Yin, C., Wang, H., Wu, X., Lan, D., Zhou, L., and Ge, C. (2023). Graph embedding-based money laundering detection for ethereum. *Electronics*, 12(14):3180.
- Manning, M., Akartuna, E. A., and Johnson, S. (2025). Opportunities to future crime: Scoping the future of money laundering and terrorist financing through cryptoassets. *Technological Forecasting and Social Change*, 210:123894.
- Pocher, N., Zichichi, M., Merizzi, F., Shafiq, M. Z., and Ferretti, S. (2023). Detecting anomalous cryptocurrency transactions: an aml/cft application of machine learning-based forensics. *Electronic Markets*, 33(1):37.
- Shojaeinasab, A. (2024). *Decoding Illicit Bitcoin Transactions: A Multi-Methodological Approach for Anti-Money Laundering and Fraud Detection in Cryptocurrencies*. Doctoral dissertation, University of Victoria.
- Vatsa, V. R. (2025). Stablecoin growth and market dynamics. Technical Report 5325570, SSRN. SSRN Working Paper.
- Verafin, N. (2024). Global financial crime report. *ABA Banking Journal summary (Jan 19, 2024)*: <https://bankingjournal.aba.com/2024/01/nasdaq-finds-scams-led-to-486-billion-in-losses-in-2023>.

## A Full Feature List

This appendix provides the complete list of 68 engineered features, categorized by their extraction logic and data type.

Feature Name	Description	Type	Source
hasKYC	Interacted with a protocol requiring KYC	Bool.	Interaction
receivedFromPayment	Received funds from a payment service	Num.	Interaction
receivedFromBet	Received funds from a betting protocol	Num.	Interaction
receivedFromCex	Received funds from a centralized exchange	Num.	Interaction
receivedFromCustody	Received funds from a cold wallet or treasury	Num.	Interaction
receivedFromDefi	Received funds from a DeFi protocol	Num.	Interaction
receivedFromDex	Received funds from a decentralized exchange	Num.	Interaction
receivedFromFlagged	Received funds from a flagged address	Num.	Interaction
receivedFromLending	Received funds from a lending protocol	Num.	Interaction
receivedFromMixer	Received funds from a mixer service	Num.	Interaction
receivedFromSC	Received funds from a smart contract	Num.	Interaction
receivedFromStake	Received funds from a staking protocol	Num.	Interaction
receivedFromSwap	Received funds from a swap protocol	Num.	Interaction
sentToBet	Sent funds to a betting protocol	Num.	Interaction
sentToCex	Sent funds to a centralized exchange	Num.	Interaction
sentToCustody	Sent funds to a cold wallet or treasury	Num.	Interaction
sentToDefi	Sent funds to a DeFi protocol	Num.	Interaction
sentToDex	Sent funds to a decentralized exchange	Num.	Interaction
sentToFlagged	Sent funds to a flagged address	Num.	Interaction
sentToLending	Sent funds to a lending protocol	Num.	Interaction
sentToMixer	Sent funds to a mixer service	Num.	Interaction
sentToPayment	Sent funds to a payment service	Num.	Interaction
sentToSC	Sent funds to a smart contract	Num.	Interaction
sentToStake	Sent funds to a staking protocol	Num.	Interaction
sentToSwap	Sent funds to a swap protocol	Num.	Interaction
usedWithAirdrop	Interacted with an airdrop participant	Num.	Interaction
usedWithDao	Interacted with a DAO address	Num.	Interaction
2ndWithMixBehaviour	Second-degree connection with mixer behavior	Num.	Derived
2ndWithMultipleSameValue	2 <sup>nd</sup> degree connection with repetitive same-value	Num.	Derived
2ndWithBet	Second-degree connection with betting wallet	Num.	Derived
2ndWithCex	Second-degree connection with centralized exchange	Num.	Derived
2ndWithCluster	Second-degree connection with clustered wallets	Num.	Derived
2ndWithCustody	Second-degree connection with cold wallet	Num.	Derived
2ndWithDefi	Second-degree connection with DeFi protocol	Num.	Derived
2ndWithDex	Second-degree connection with decentralized exchange	Num.	Derived
2ndWithFlagged	Second-degree connection with flagged address	Num.	Derived
2ndWithLending	Second-degree connection with lending protocol	Num.	Derived
2ndWithMixer	Second-degree connection with mixer	Num.	Derived
2ndWithOver1k	Second-degree connection with >1k transfer	Num.	Derived
2ndWithOver5k	Second-degree connection with >5k transfer	Num.	Derived

Feature Name	Description	Type	Source
2ndWithOver10k	Second-degree connection with >10k transfer	Num.	Derived
2ndWithPayment	Second-degree connection with payment wallet	Num.	Derived
2ndWithProxy	Second-degree connection with proxy wallet	Num.	Derived
2ndWithSC	Second-degree connection with smart contract	Num.	Derived
2ndWithSingleFrom	Second-degree with single outgoing wallet	Num.	Derived
2ndWithSingleTo	Second-degree with single receiving wallet	Num.	Derived
2ndWithStaking	Second-degree connection with staking protocol	Num.	Derived
2ndWithSwap	Second-degree connection with swap protocol	Num.	Derived
3rdWithFlagged	Third-degree connection with flagged wallet	Num.	Derived
circleDetected	Reciprocal transfers within 24 hours	Num.	Derived
clusterScore	Number of flagged direct connections	Num.	Derived
hasMixerBehaviour	Imbalance between sent and received volumes	Num.	Derived
hasProxyBehaviour	Received and sent same amount in 24h	Num.	Derived
isPartOfClusterFrom	Sends funds with same value and destination	Bool.	Derived
isPartOfClusterTo	Receives funds with same value and origin	Bool.	Derived
receivedFromProxy	Received funds from proxy wallet	Num.	Derived
sentToProxy	Sent funds to proxy wallet	Num.	Derived
receiveMulSameValue	Received multiple transfers with the same value	Num.	Transfer
receiveSingleFrom	Multiple transfers from a single address	Num.	Transfer
sentMultipleSameValue	Sent multiple transfers with the same value	Num.	Transfer
sentToSingleAddress	Multiple transfers to a single address	Num.	Transfer
transferOver1k	Transfer over 1,000 USD-equivalent	Num.	Transfer
transferOver5k	Transfer over 5,000 USD-equivalent	Num.	Transfer
transferOver10k	Transfer over 10,000 USD-equivalent	Num.	Transfer
highFrequency	More than 10 transfers in the same day	Num.	Temporal
isLongTermWallet	Active across more than 3 months	Bool.	Temporal
isVerifiedContract	Smart contract with verified source code	Bool.	Direct
isWallet	Address has no bytecode (EOA)	Bool.	Direct

**Table 8:** Engineered features capturing wallet behaviors and interactions.

## B Hyperparameter Optimization

To ensure fair comparison and reproducibility, we performed a full *Grid Search* with 5-fold cross-validation on the training set to identify the optimal hyperparameters for each model. The optimization objective was to maximize the Macro-F1 score, ensuring a balanced trade-off between precision and recall across the imbalanced classes.

For LR, we optimized the regularization strength ( $C$ ) and penalty type using the `saga` solver, which was selected a priori to support efficient convergence on large datasets with  $L_1$  penalties. For tree ensembles, which include both bagging (RF) and boosting (XGBoost, LightGBM, CatBoost) techniques, we targeted structural parameters governing tree complexity (depth, splits) and ensemble size (estimators, learning rate).

Tables 9, 10, and 11 detail the search spaces defined for the grid, the rationale behind each parameter, and the final optimal values selected for the reported results.

Parameter	Search Grid	Best Value	Design Rationale
$C$ (Inverse Reg.)	$[10^{-3}, 10^1]$	10	Controls model complexity ( $1/C$ ); higher values reduce regularization.
Penalty	$\{L_1, L_2\}$	$L_1$	$L_1$ promotes feature sparsity; $L_2$ prevents large weights.

**Table 9:** Logistic Regression optimization. The `saga` solver was fixed for all experiments.

Parameter	Search Grid	Best Value	Design Rationale
$n_{\text{estimators}}$	[100, 500]	400	Number of trees; higher improve stability.
min_samples_split	[2, 10]	5	Samples required to split an internal node.
min_samples_leaf	[2, 5]	2	Samples required at a leaf node (smoothing).
max_features	$\{\text{sqrt}, \log 2\}$	sqrt	Fixed to decorrelate trees in the ensemble.

**Table 10:** Random Forest (Bagging) optimization settings.

Parameter	Search Grid	Best Values (XGB/LGBM/CatB)	Rationale
$n_{\text{estimators}}$	[100, 700]	200 / 640 / 300	Boosting rounds; trade-off between accuracy and speed.
Learning Rate	[0.01, 0.3]	0.1 / 0.01 / 0.25	Step size; lower values require more estimators.
Max Depth	[3, 10]	9 / 10 / 7	Controls interaction complexity and overfitting.
Subsample	[0.8, 1.0]	0.8 / 0.8 / -	Fraction of data used per iteration.
Colsample	[0.8, 1.0]	0.8 / 0.8 / -	Fraction of features used per tree.

**Table 11:** GBMs optimization settings. Note: CatBoost uses default sampling strategies; specific depth and iteration parameters were mapped to their framework equivalents.

## C Full Three Classification Performance Result

This appendix details the comprehensive performance metrics for the multiclass classification task. It breaks down the AUROC, precision, recall, and F1 scores for each evaluated model across the three distinct behavioral classes: *Normal* (0), *Cybercrime* (1), and *Blocklisted* (2). This granular view highlights the superior capacity of tree ensembles to distinguish between complex laundering schemes and static blocklisted entities compared to linear baselines.

Model	Class	AUROC	Precision	Recall	F1	Support
Logistic Regression	0	0.9453	0.7877	0.9988	0.8807	1623
	1	0.9351	0.9375	0.7614	0.8403	1182
	2	0.9353	0.8773	0.4896	0.6285	482
Random Forest	0	0.9994	0.9951	1	0.9975	1623
	1	0.9990	0.9817	0.9768	0.9792	1182
	2	0.9946	0.9395	0.9355	0.9375	482
CatBoost	0	0.9990	0.9927	1	0.9963	1623
	1	0.9991	0.9873	0.9831	0.9852	1182
	2	0.9943	0.9579	0.944	0.9509	482
LightGBM	0	0.9989	0.9927	1	0.9963	1623
	1	0.9993	0.9864	0.9805	0.9835	1182
	2	0.9947	0.9518	0.9419	0.9468	482
XGBoost	0	0.9987	0.9927	0.9994	0.996	1623
	1	0.9992	0.9889	0.9805	0.9847	1182
	2	0.9942	0.9501	0.9481	0.9491	482
DNN	0	0.9896	0.9100	0.9986	0.9522	1623
	1	0.9518	0.9477	0.9319	0.9390	1182
	2	0.9436	0.8581	0.6208	0.7211	482
GNN	0	0.9735	0.7725	0.9601	0.8557	1623
	1	0.9647	0.9010	0.7366	0.8109	1182
	2	0.9667	0.9592	0.6131	0.7481	482

**Table 12:** Detailed multiclass performance metrics by model. The labels correspond to Normal (0), Cybercrime (1), and Blocklisted (2) entities.